Endres, H., Samiee, R., Lohr, T., Krawczyk, C. M., Tanner, D. C., Trappe, H., Thierer, P. O., Oncken, O., Kukla, P. A. (2008): Quantitative fracture prediction from seismic data. - Petroleum Geoscience, 14, 4, 369-377

DOI: 10.1144/1354-079308-751

Quantitative fracture prediction from seismic data

H. Endres[1,2,*], T. Lohr[4], H. Trappe[1], R. Samiee[3], P. O. Thierer[1], C. M. Krawczyk[4,5], D. C. Tanner[2,5], O. Oncken[4] and P. A. Kukla[2]

[1]*TEEC, Burgwedelerstr. 89, D-30916 Isernhagen HB, Germany*
[2]*Geological Institute, RWTH Aachen, Wuellnerstr. 2, D-52056 Aachen, Germany*
[3]*RWE Dea AG, Ueberseering 40, D-22297 Hamburg, Germany*
[4]*GeoForschungsZentrum Postdam, Telegrafenberg, D-14473 Potsdam, Germany*
[5]*Institut für Geowissenschaftliche Gemeinschaftsaufgaben (GGA), Stilleweg 2, D-30655 Hannover, Germany*
[*]*Corresponding author (e-mail: endres@teec.de)*

ABSTRACT: This paper presents results obtained from an area located east of Bremen, Germany, where gas is produced from a deep Rotliegend sandstone reservoir. Faults, fractures and associated deformation bands at reservoir depth have an important influence on the productivity of the gas field as fractures are cemented and tight and may act as permeability barriers. This contribution comprises the development of new coherency tools to better image sub-seismic faults and lineaments from seismic data, and the development of fracture attributes in order to quantify fracturation and its areal distribution.

The fractal behaviour of faults was used to establish a relationship between coherency processed seismic data and borehole images at log scale. The 'fractal dimension' (FD) of the length of a fault population can be interpreted as a characteristic parameter describing local geology in terms of fracturation. Calculating FD for each point of a seismic grid yields an areal distribution of this value. Correlating seismic-derived FD values and fracture populations derived from borehole images defined a linear relationship which can be used to forecast the distribution of sub-seismic fractures and deformation from seismic data.

KEYWORDS: *Rotliegend sandstones, quantitative fracture prediction, sub-seismic faults, seismic data, coherency analysis, fractal dimension, fracture density*

INTRODUCTION

Sedimentary basins evolve following a variety of spatial and temporal processes, and exhibit a complex pattern of structural and deformational features and styles (Allen & Allen 1990). The sedimentary North German Basin (NGB) has been affected by a variety of deformational events since Permian time (Ziegler 1990; Scheck & Bayer 1999; Kockel 2002; Kossow & Krawczyk 2002). These events vary primarily in the magnitude of deformation and in the strain accumulation in space and time. Large-scale subsurface deformation causes structures identified by seismic data. However, small-scale subsurface deformation also accommodates a significant amount of the total strain, the so-called sub-seismic deformation (Scholz & Cowie 1990; Marrett & Allmendinger 1991). Small-scale fractures and faults can influence the reservoir characteristics of a sedimentary basin strongly. They can have a considerable lateral continuity and therefore significantly compartmentalize areas and reservoirs (Mauthe 2003). Small-scale tectonic elements (Fig. 1) could act as conduits for mineralizing fluid flow and dramatically reduce porosity and permeability (Walsh *et al.* 1998). The presented reservoir faults and fractures are typically cemented by quartz and calcite. The fractures act as permeability barriers and typically coincide with poor reservoir quality.

This study of seismic and sub-seismic deformation in the NGB aims to predict the quantitative fracture density from seismic data. Structural elements, such as faults and fractures, as well as deformation information, have been identified and classified using coherency processing, geostatistical analysis and core data. The 3D structural interpretation of seismic and well data is summarized by Lohr *et al.* (2007). This paper focuses on new approaches to quantitative fracture prediction from seismic data using advanced coherency processing techniques in context with fracture data analysis from borehole images in a North German gas field.

TECTONIC SETTING

The NGB developed on crystalline basement of varying Precambrian age (Tanner & Meissner 1996; Krawczyk *et al.* 1999). It forms part of the Southern Permian Basin, a large intracontinental basin system that varies in width between 300 km and 600 km, and which extends from the North Sea to Poland (see review of Pharaoh 1999; Fig. 2). Post-Variscan rifting produced a system of graben and half-graben, affecting Carboniferous to Permian rocks (Betz *et al.* 1987; Brink *et al.* 1992; Kockel 2002). The basin contains Mesozoic to Cenozoic sediments of up to 10 km in thickness (Plein 1995; Baldschuhn *et al.* 1996). Thermal subsidence continued until the Triassic and

Petroleum Geoscience, Vol. **14** 2008, pp. 369–377
DOI 10.1144/1354-079308-751

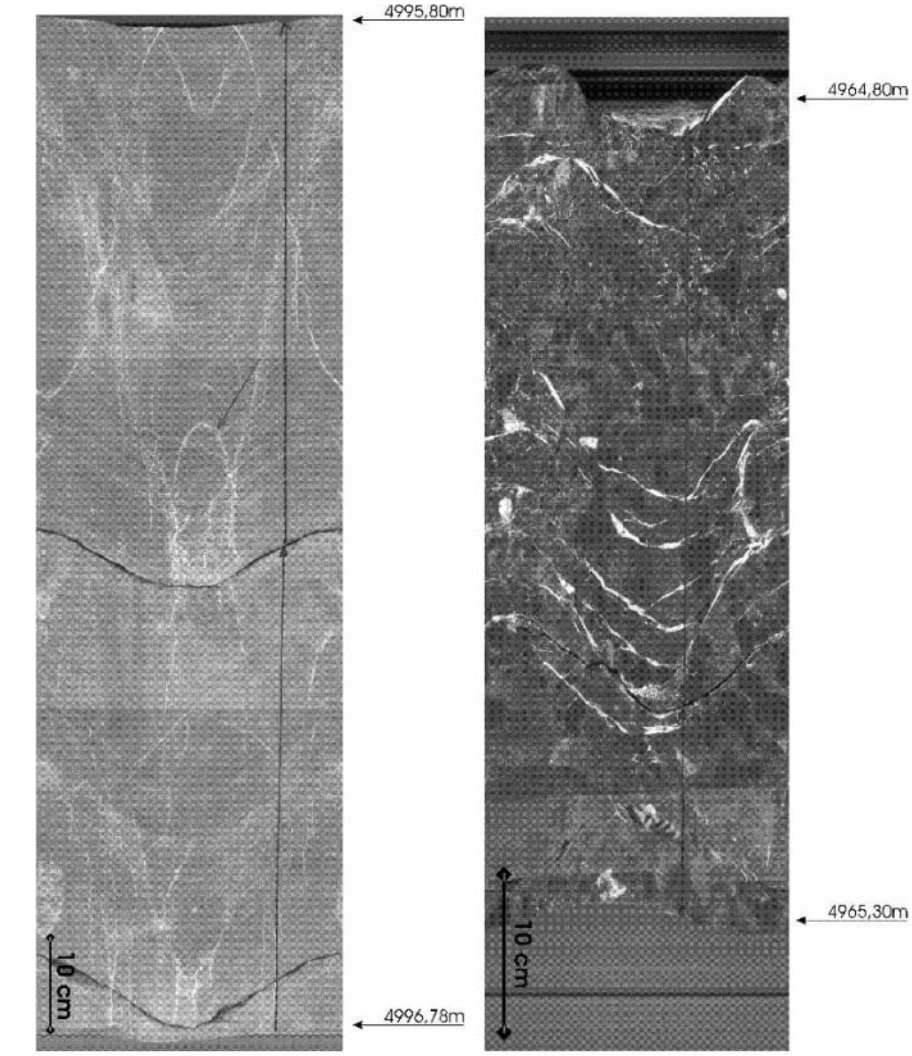

Fig. 1. Two whole core scans. (**a**) Aeolian sandstone; the arrow points to deformation bands and/or quartz-filled fractures. (**b**) Proximal alluvial fan deposit. The arrow points to fractures that were filled later with breccias and by calcite mineralization.

several pulses of uplift occurred from the Jurassic onwards (Schwab *et al.* 1982; Kossow *et al.* 2000).

This paper focuses on a producing gas field east of Bremen (NW Germany) where faults and fracturation play a major role in gas productivity. The area is characterized by four Zechstein (Upper Permian) diapirs, rooted above the Rotliegend (Lower Permian) at depths between 4500 m and 4800 m (e.g. seismic section in Fig. 3; Lohr *et al.* 2007). Normal faults with displacements varying from 100 m to 300 m at Top A2 (Lower Zechstein) affect the area. Orientation and kinematics indicate an extensional stress regime within the Rotliegend and Lower Zechstein (Lohr *et al.* 2007). Jurassic transtension and Upper Cretaceous inversion involved mainly the basement and are associated with uplift of the Upper Permian/Lower Zechstein horizons (Fig. 3). Thus, fault activity and kinematics varied strongly in the study area in space and time.

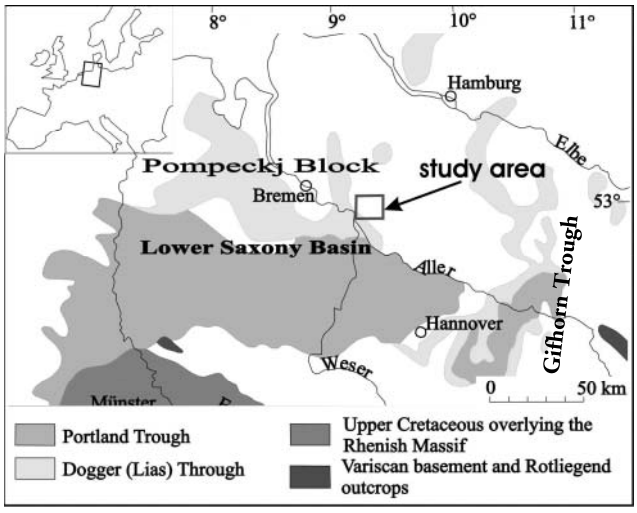

Fig. 2. Regional overview map (after Betz *et al.* 1987), with main tectonic elements. Location of study area is marked by rectangle and arrow.

DATABASE

All borehole-related and seismic data were made available from gas exploration and production, provided by RWE Dea AG Hamburg. The database consists of a 3D pre-stack depth-migrated reflection seismic dataset (PSDM) with an inline and crossline spacing of 25 m and a sample rate of 4 ms. It covers an area of about 10 × 10 km and images depths down to the Carboniferous (*c.* 7200 m). The resolution is determined by the above values of inline and crossline spacing, data bandwidth and target depth. In general, the horizontal resolution will increase using a PSDM dataset compared to an unmigrated dataset. Faults and fractures must be detected on at least four

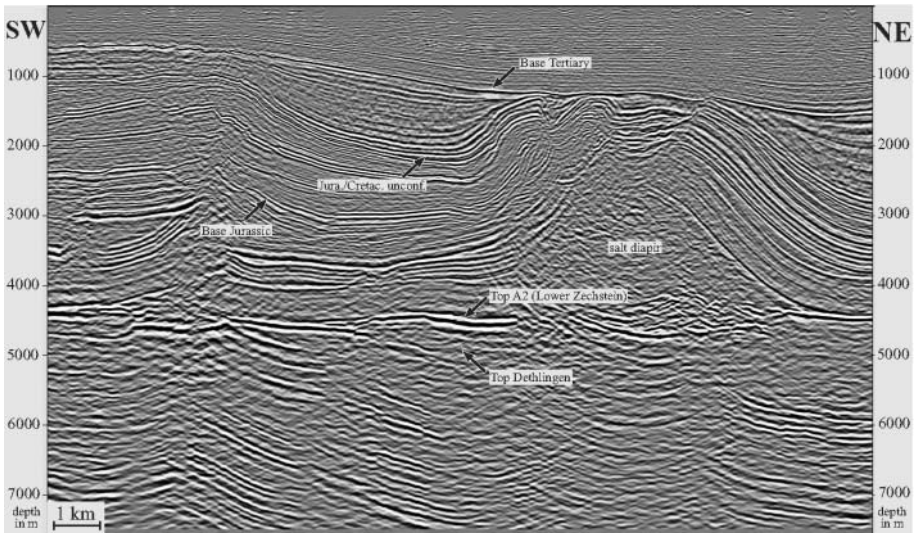

Fig. 3. Depth-migrated reflection seismic SW–NE traverse through the study area. The basement shows predominantly extensional structures. Mesozoic horizons are disturbed by normal faulting and partly associated block rotation. Folds at the outer rim of the diapir probably are related to transpressional strike-slip faulting (modified after Lohr *et al.* 2007).

inline or crosslines, which leads to a minimum horizontal feature length of 100 m, greater than the seismic data resolution.

Thirteen wells provide information on petrophysical data, core sections, log curves and borehole images, of which only the latter are unavailable for wells B and K. The borehole images are logged using the Schlumberger Formation-Micro-Imager (FMI) (Goodall *et al.* 1998) and Formation-Micro-Scanner (FMS) (Ekstrom *et al.* 1987) micro-resistivity tools. The FMI information was provided for this project. As not all core sections from reservoir depth are of the same length, all FMI fracture density values were normalized to a reference length of 300 m.

COHERENCY PROCESSING

The objective of coherency processing is to improve the resolution of the structural image and to allow a better identification of subtle lineaments in the study area. Faults, fractures and other lineaments caused by lithology changes, fluid contacts, gas–water contacts etc. can be detected using advanced coherency processing algorithm workflows (Trappe *et al.* 2000; Trappe & Hellmich 2003). The coherency analysis can be carried out in either the time or depth domain. As the PSDM dataset was provided, the coherency analysis was carried out in the depth domain, but the technique would be the same for processing in either time or depth.

For each sample of a seismic data volume, the technique calculates the similarity (coherency) of the surrounding seismic data. Areas of constant lateral lithology cause similar seismic signals, which lead to high lateral continuity values. In contrast to this, geological features, such as fractures and faults, decrease the lateral similarity of the seismic data in the local neighbourhood. The results of the coherency processing are stored in three data volumes, which contain the three attributes: maximum coherency, associated local dip and azimuth. These volumes have the same size and geometry as the analysed volume. They can be interpreted in the usual way by displaying time or horizon slices and profiles of each volume (Fig. 4a). In addition, the three attributes can be merged into one IHS (Intensity, Hue and Saturation) display (e.g. Fig. 4b). This display provides a better resolution compared to the conventional coherency display (compare Figs 4a and b). In order to display the lineaments better, the IHS colour wheel can be rotated. This results in changing colour codings of dip directions and coherency surfaces to identify subtle lineaments more accurately (Figs 4c and f).

Supplementing well-established similarity measure techniques from image processing (e.g. cross-correlation, dispersion or fractal dimension; Aminzadeh 1987; Yilmaz 1987), additional new coherency algorithms are introduced here, which improve the identification of subtle tectonic lineaments. The 'shaded relief' coherency operator considers different intensities of reflected light. The intensities are a function of the light-source direction (analogous to the Sun) and the local orientation of the analysed sub-volume surface. The position of the light source (elevation above the horizontal and azimuth) can be varied to obtain optimal results. Similar seismic patterns show similar reflectivity values, highlighting reservoir heterogeneities and tectonic elements. High reflectivity values correspond to a high conformity of neighbouring seismic traces (light colours). Low agreement of seismic patterns is represented by low reflectance values or dark colours. Thus, details of geological structure and the orientation of faults and folds are enhanced (Fig. 4d). 'Structural entropy' is a measure of local discontinuity on a scale from zero to one. It indicates the degree of discontinuity within a given sub-volume of a seismic dataset. By transforming the 3D seismic data into a structural-entropy volume, subtle tectonic elements such as faults and folds can be highlighted (Fig. 4e).

TECTONIC LINEAMENTS IN THE STUDY AREA

The coherency analysis focused on the Top A2 horizon, Upper Permian. The main tectonic elements in the region are horst and graben and half-graben structures, easily detected in the conventional coherency display obtained from a standard coherency processing. Continuous fault traces, up to 10 km long, occur throughout the study area. The highly unstructured area found in the northeastern part of the coherency map is due to the presence of a salt diapir (top left in each plot in Fig. 4).

Since there are several wells concentrated in the study area, advanced coherency analyses (IHS, shaded relief, structural entropy) were carried out and the results calibrated with the corresponding well data. Whereas the Zechstein Top A2 horizon appears more or less homogeneous (white-greyish patches) in most of the study area, the advanced processing reveals many small-scale features (Fig. 4), which are not detectable in either the seismic image or the conventional coherency display. Arrows in Figure 4 indicate the significantly

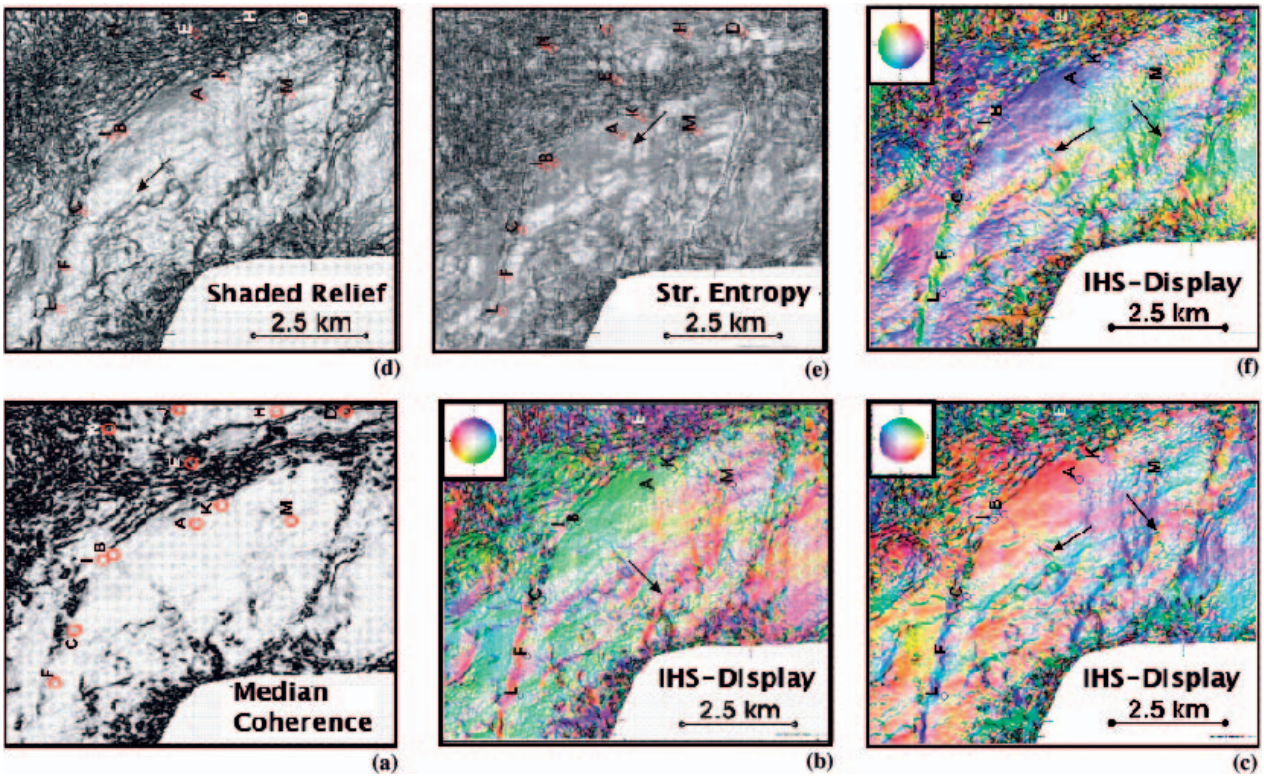

Fig. 4. Results of coherency processing of the Top A2 horizon: (**a**) standard coherency display; (**b**) IHS display, illumination: 0°; (**c**) IHS display, illumination: 120°; (**d**) results from shaded-relief calculations; (**e**) structural-entropy image; (**f**) IHS display, illumination: 240°, arrows point to additional tectonic elements, letters label well sites. North is to the left in all plots.

improved imaging of lineaments due to the application of better coherency techniques. In addition to the main tectonic lineaments, which have the strongest continuity, more small-scale features are interpreted crossing the main features at a low angle (Fig. 5). The results provide a greater fault density than could have been inferred from a conventional amplitude image.

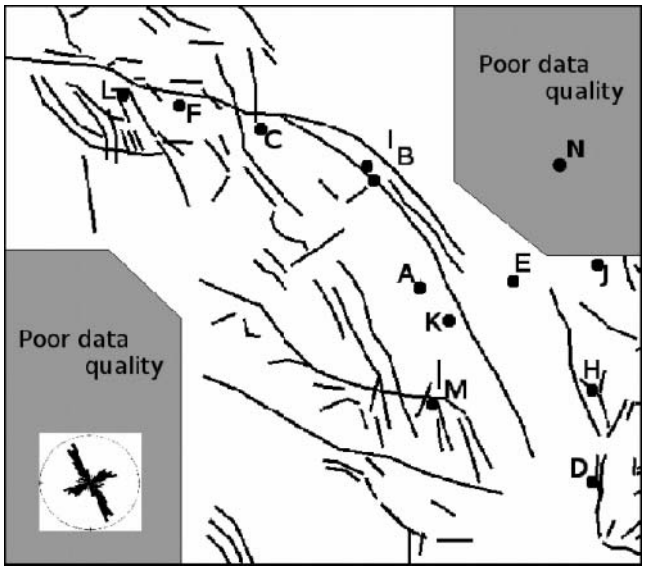

Fig. 5. Interpreted faults in the study area based on coherency processing (cf. Fig. 4). Inset: rose diagram illustrating the orientation of interpreted fractures and fault. A well-defined NW–SE fault strike trend is evident on both small-scale borehole image data and large-scale seismic images.

CORRELATION WITH BOREHOLE IMAGE DATA

Parallel to the seismic and coherency interpretation, results of borehole images were provided by RWE Dea AG, having been analysed with respect to fault and fracture patterns, cementation, orientation and density, using core data to support the image log interpretation. The FMS/FMI borehole imaging tools use arrays of pad-mounted, button electrodes, at 2.5 mm vertical and horizontal spacing, to provide a continuously orientated map of the electrical conductivity of the borehole wall. Objects are fully resolved to 5 mm but smaller features, such as fractures, are detectable providing there is a resistivity contrast. The resulting images provide dip and azimuth of planar conductivity contrasts that correspond to bedding in sedimentary rocks or to faults, fractures and veins. The colour code is standardized such that light and dark colours represent high and low formation resistivities, respectively. In general, the fractures in the borehole images of the study area can be classified into two types (Fig. 6). Highly resistive fractures appear as bright features which are discordant to bedding. These fractures may represent closed mineralized fractures (highly resistive minerals such as calcite and dolomite) or small-scale deformation bands. Low resistive (conductive) fractures appear on images as dark features, which are discordant to bedding.

The borehole image corresponds to an unwrapped cylinder (Fig. 6). The well analysed here contains several isolated fractures and several small faults which consist of a number of closely spaced individual fractures. The majority of fractures show a well-defined NW–SE strike direction, with dip directions towards both the NE and SW, but a subset of the fractures is perpendicular and strikes in an ENE–WSW direction. Dip angles are generally steep, and lie between 65° and

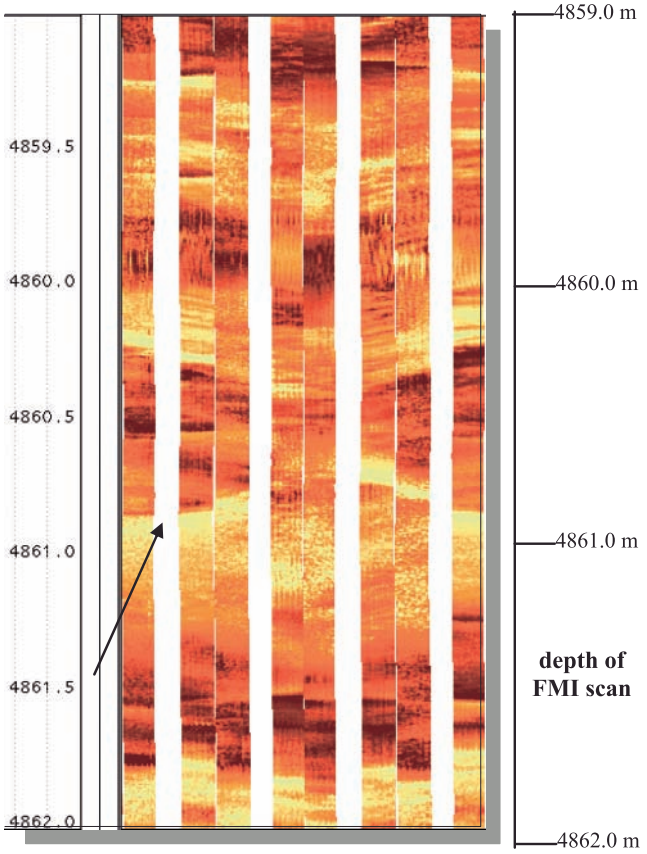

Fig. 6. Borehole image corresponds to an unwrapped cylinder representing the borehole. Note the presence of fractures (arrow) striking NW–SE and dipping SW.

90°. The corresponding rose diagram summarizes the orientation of interpreted fractures and faults based on the borehole image analyses (Fig. 5, inset). Comparison with the faults interpreted from coherency maps points out the good correlation between the coherency and borehole image results. The well-defined NW–SE strike direction of faults can be seen consistently in both types of data.

FAULT ATTRIBUTE ANALYSES

The main features of the fault system in the study area were interpreted at the Zechstein Top A2 horizon. First, on two-way travel time maps and, secondly, with normal coherency and IHS horizon slices. For quality control of fault interpretation on horizon slices, normal amplitude, coherency, dip and azimuth cross-sections were taken into account. To be interpreted as a fault, tectonic features identified on horizon slices also had to be detected on at least several inlines or crosslines on the normal amplitude and/or coherency cross-sections. In addition, only tectonic elements with a vertical length in the cross-section of at least 20 ms, which corresponds roughly to 80 m, were considered. After all faults and lineaments had been interpreted (see Fig. 5), a fault attribute analysis was performed, yielding fault density maps (Fig. 7). The fault density is calculated for each point on the map using an areal search window and performing an image analysis. For this purpose, different window sizes were tested in order to achieve stable results. The edge length of this rectangular search window was 1.8 km for all attributes calculated. The attributes were: (1) density by count (Fig. 7a), which counts the number of faults within the search area; (2) density by length (Fig. 7b), which evaluates the

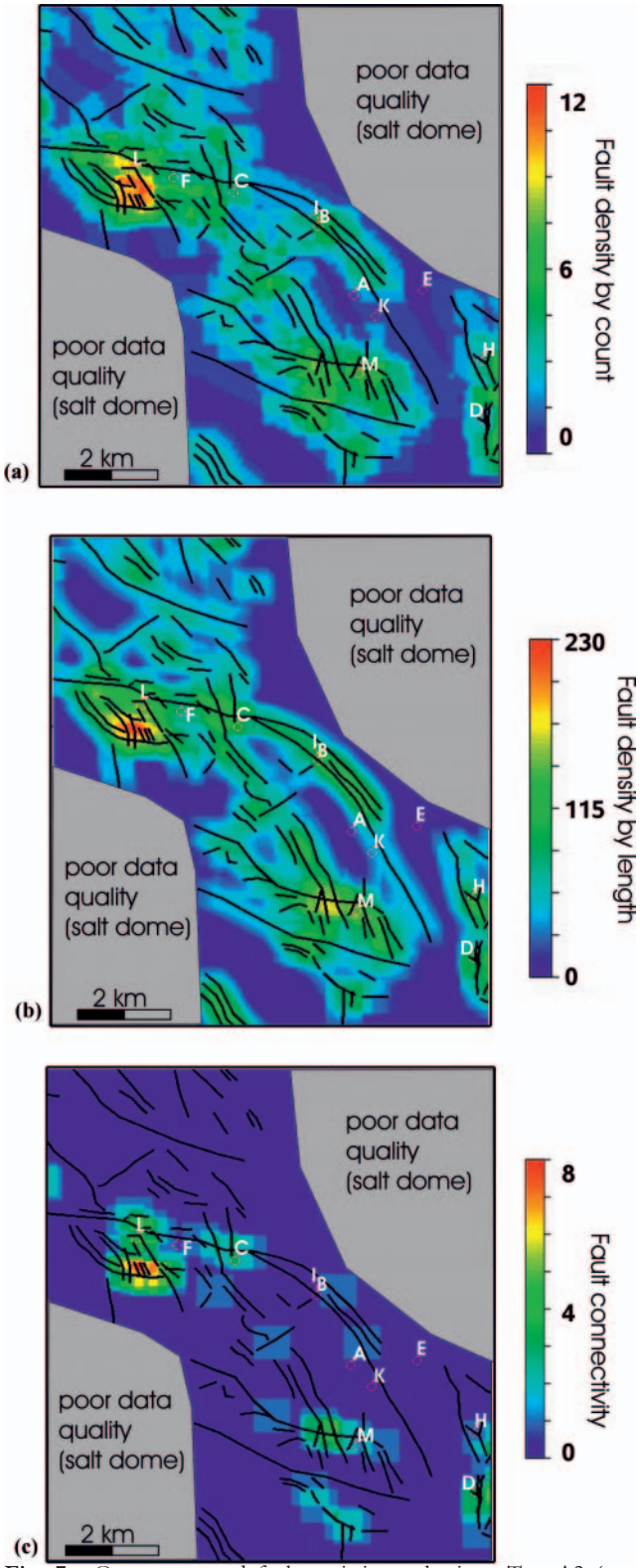

Fig. 7. Occurrence and fault statistics at horizon Top A2 (area 10 × 10 km). Interpreted faults are according to Figure 5. (**a**) Fault density by count; (**b**) fault density by length; (**c**) fault connectivity. Note the areas of high fault density (red, A and B) and high fault connectivity (red, C) in the vicinity of well L.

total length of all faults/lineaments intersecting the search window; and (3) connectivity (Fig. 7c), which gives the degree of interconnection – the number of intersections within the search window of the interpreted faults and lineaments.

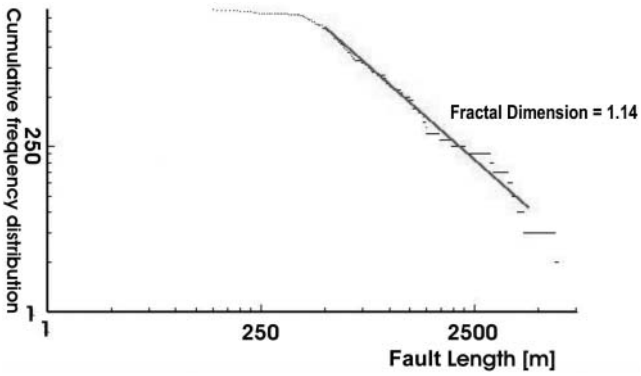

Fig. 8. Fractal dimension of cumulative fault length: straight line indicates that the length distribution follows a power law. Negative slope = fractal dimension (FD).

DENSITY AND CONNECTIVITY OF FAULTS

The fault-density maps reveal high fault-density values in the NW and SE quadrants, reaching values higher than ten per unit, where an average between one to two per unit is generally found (Fig. 7a). By coincidence, the density by length attribute map also shows its maxima in the NW and SE quadrants, respectively. For this fracture attribute, maximum values ranging up to more than 200 per unit were found, where an average for the whole dataset is less than 30 per unit (Fig. 7b). The absolute values presented give an overview of the data range. These relative deviations are important because they show the variability in terms of the attribute described. The density maximum in the NW coincides with the maximum of connectivity (Fig. 7c). The overlay of the main tectonic elements interpreted in the region (see Fig. 5) shows that these attribute maxima are found in the vicinity of large-scale, continuous, W–E-trending faults. These are normal faults bounding the main half-graben in the region. Continuous NW–SE-trending faults in the centre of the investigated volume enlarge the fault density at that location (Fig. 7a and b), but they do not enhance the connectivity there (Fig. 7c).

FRACTAL DIMENSION

Besides other fracture attributes, such as orientation, density or spatial distribution, the length was analysed in greater detail. In general, if the ratio of 'long' and 'short' fractures is constant over different scales, it follows the law of scale-invariance, that is to say the relationship is fractal. This means that there is a power-law relation between those 'long' and 'short' fractures. Results are presented typically in log–log diagrams, where length populations are plotted as a cumulative frequency distribution (Fig. 8). The straight line indicates that the length distribution follows a power law. Its exponent, -a, is the 'fractal dimension', FD.

The calculation of the FD value (Fig. 8) is based on the seismic data. For the whole area it yields a number of 1.14, which represents an average value characteristic for the area of interest. In general, a higher value indicates a higher relative frequency of 'short' faults than does a small number. When calculating the FD value for the single data points covering the working area, the lower size of that area must be limited, otherwise the calculated FD value becomes unstable due to few data inside the calculation area. For the present dataset, it was found that a grid of 1.5 km spacing gave the best result (Fig. 9). At the locations of well E, J and N, no FD values could be calculated due to poor seismic data quality. Despite the lack of FD values it is still possible to estimate seismic fault or fracture densities in the vicinity of these wells, although with a high degree of uncertainty.

Two domains were observed with higher than average FD values in which the occurrence of short faults is predominant. They are situated in the southeastern (well M) and northwestern (well L) parts of the study area, respectively.

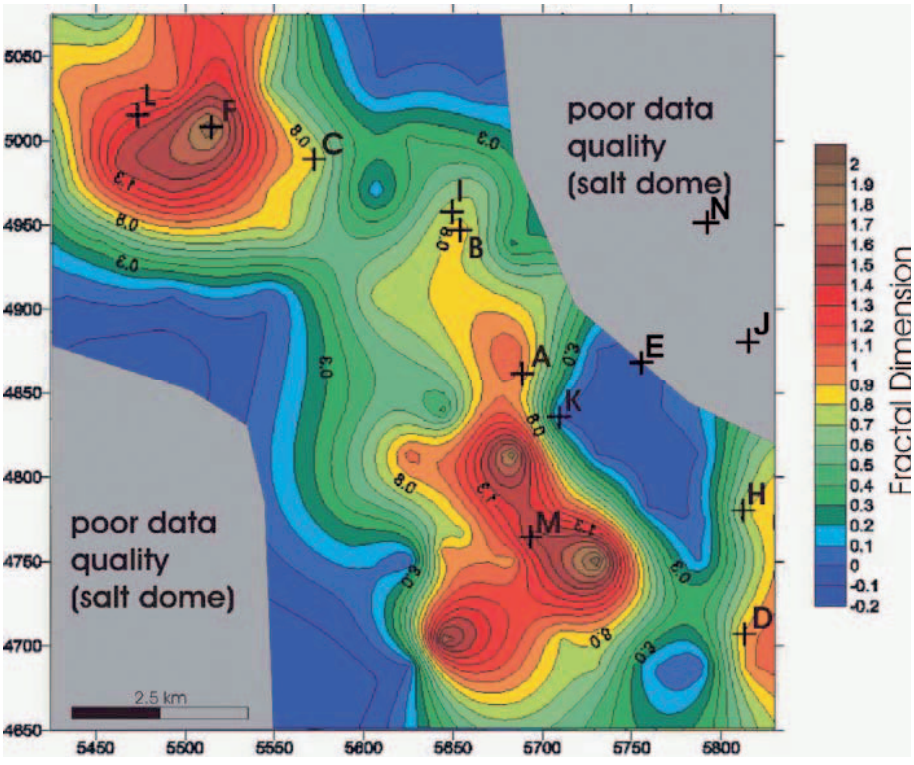

Fig. 9. FD distribution calculated from seismic data with 1.5 km grid size using kriging algorithm. FD maxima (predominantly short faults) are observed in the NW and SE parts of the study area.

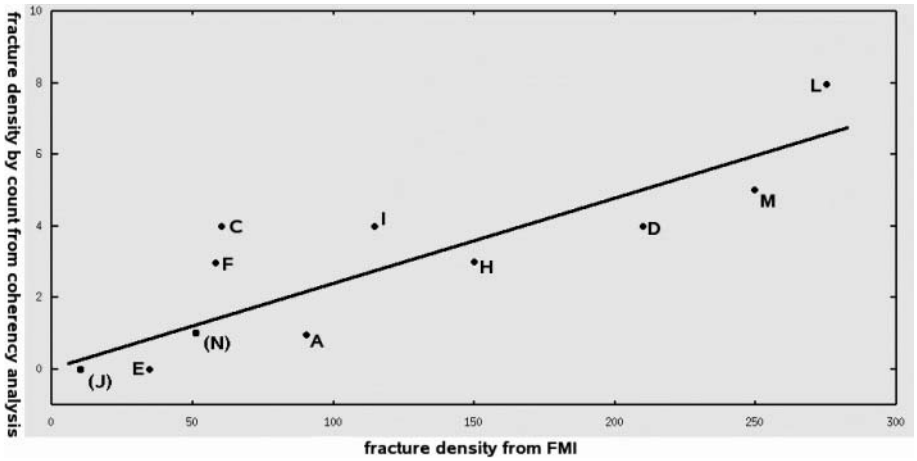

Fig. 10. Relationship between fault/fracture densities at seismic scale (cf. Fig. 7a) and at borehole image scale (cf. Fig. 6). The linear relation emphasizes the good correlation of measured and calculated fracture densities at different scales. Wells J and N are in parentheses to indicate high uncertainties in their seismic fracture densities. They were not used in the regression.

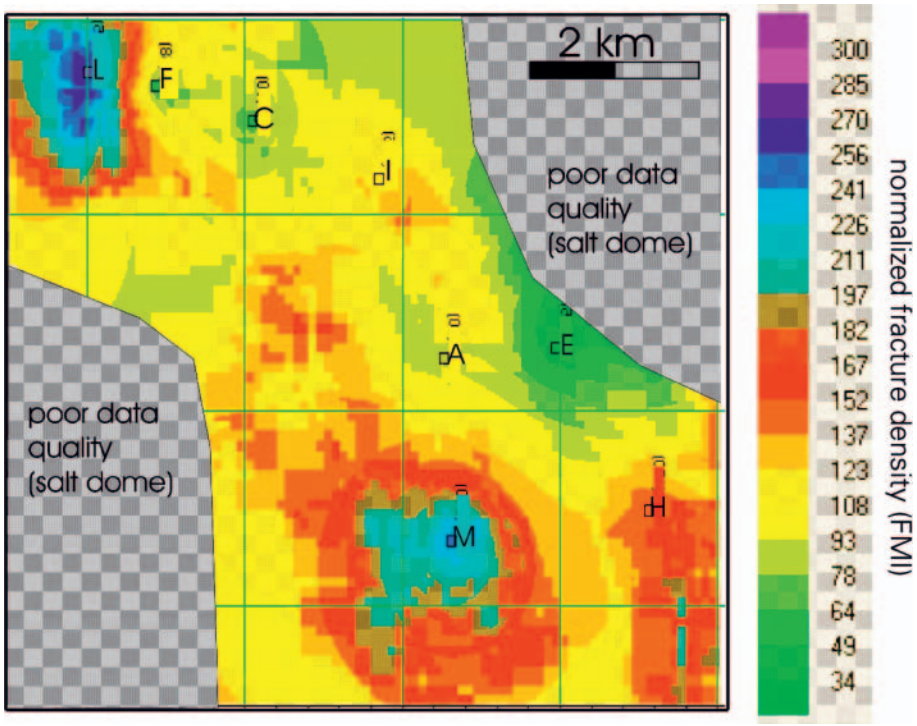

Fig. 11. Distribution of normalized fracture data based on borehole images (cokriged map, area 10 × 10 km).

GEOSTATISTICAL ANALYSES

The geostatistical analyses aim to predict fault/fracture densities in undrilled areas at sub-seismic scale within the Rotliegend reservoir. Since proximity to faults/fractures could be a factor in reducing porosity and permeability, it is necessary to establish the relation between the fault/fracture density derived from borehole images (millimetre to centimetre scale) and fault/fracture density derived from coherency analyses (decametre scale). For this reason, the normalized FMI data of the sandstone reservoir were analysed for 11 wells in terms of fault/fracture pattern and density. The resulting fault/fracture density from image log data varies between zero and 275 counts in the study area (data provided by RWE Dea AG). High fracture density values up to 275 counts are found in an elongated, NW–SE-striking area.

The relationship between fault density at seismic scale (see Fig. 7a) and fracture density at borehole image scale is important. The regression line (Fig. 10) serves furthermore as the basis for the geostatistical analysis. Although wells N and J are located inside the area of poor data quality, which is indicated by the parentheses, they fit the general trend of the regression line, although they have not been used in the regression because of their high uncertainty in seismic fracture density.

Two approaches, collocated cokriging and Gaussian simulation, were performed. Both methods show lateral variations of the normalized fracture density or, in other words, the predicted distribution of fault/fracture density at borehole image scale (Figs 11, 13).

The cokriging algorithm (Deutsch & Journel 1992) uses the given borehole image data at well locations. Interpolation between wells uses the seismic coherency information while taking into account the relationship given in Figure 10. This approach results in a map that illustrates the expected areal distribution of fault/fracture density at borehole scale (Fig. 11). The prediction reveals three areas, extending at kilometre scale, with high fracture densities. A medium density value is observed in the centre of the analysed volume. This correlates well with the results from seismic interpretation (Figs 5, 7).

Further validation concerning fracturation interpolation is based on a crossplot of FD values from seismic coherency data against image log fracture density for the eight wells where both

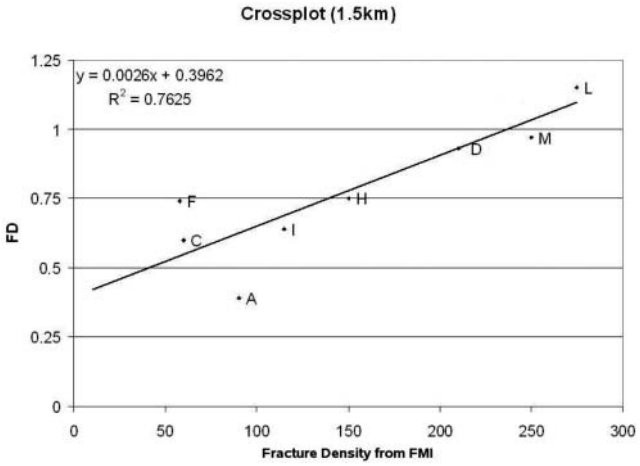

Fig. 12. Gaussian simulation probability map for low fracture densities. Green/yellow colours represent areas of low probability. These areas are, therefore, of high fracture density and thus interpreted to have lower reservoir qualities due to the sealing effect of the fracture cementation by quartz and calcite.

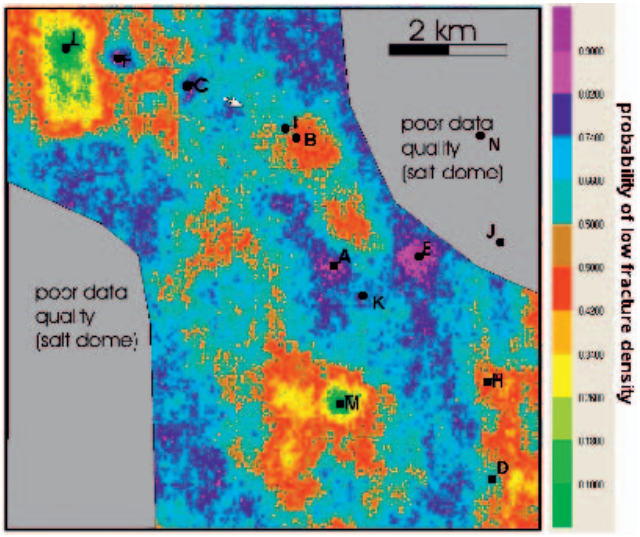

Fig. 13. Crossplot of fractal dimension of seismic interpreted faults and borehole fracture image data. It shows their linear relationship with a regression coefficient of *c.* 0.76. Wells B and K do not provide image log data and FD values were not estimated for wells E, J and N.

estimates are available. They also show good agreement; correlation based on linear regression is given with an error-variance R^2 of approximately 0.76 (Fig. 13).

Gaussian simulation (Deutsch & Journel 1992) is a procedure for predicting the fault/fracture probability between wells. Thus, it highlights the uncertainty of the information available. In this study, Gaussian simulation was performed on the basis of the cokriging result and the available areal distribution of the associated cokriging error. Image log fault/fracture densities of less than 130 counts are defined as low fracture density areas. The resulting map (Fig. 13) shows a spatially distributed pattern of high probabilities of these low fracture areas (Fig. 13, blue/pink colours). Close to the locations of wells L and M, the probability of a low fracture density is almost zero (Fig. 13, green/yellow colours), which fits the high image log fracture densities in both these wells.

In general it is observed that the well locations trend NW–SE. Consequently, a high degree of reliability is expected along this 135° trend-line with good resolution. A lower reliability in terms of resolution is expected perpendicular to the above-mentioned trend.

SUMMARY AND CONCLUSION

Basin studies with analysis of seismic and sub-seismic deformation require a very high fault resolution to link seismic results with well data. Advanced coherency algorithms increased the resolution of the seismic data and revealed additional small-scale lineaments. Comparison between borehole images and coherency results shows a good correlation between these two methods that operate on different scales. The combination of coherency results, core and image log data, linked to the FD analysis, proves to be a good method for the characterization of fault damage zones.

The presented results coincide with the methodically independently achieved results of numerical fracture modelling published by Lohr *et al.* (2007). They deduced that a maximum magnitude in strain increases with an increasing fault displacement. In accordance, the fracture density as well as the size of the fractured area increased from well A to well D.

In the future, calibration of the coherency results against borehole images and core data is recommended to provide a benchmark for the quantification of fracture studies in undrilled areas and uncored intervals. These results can be used to analyse possible relationships between the reservoir quality of wells and fault distribution.

An example was presented where faults and fractures decrease the reservoir quality due to cementation. Of course, the presented technique can be applied to uncemented fault and fracture systems that will increase reservoir quality.

The authors thank RWE Dea AG, Hamburg for providing a high-quality seismic dataset and corresponding drill-hole information. Reinhard Gaupp (Jena University) is thanked for discussion and field guidance into the sedimentary aspects of the Rotliegend of the North German Basin. This study has been funded by the Deutsche Forschungsgemeinschaft within the SPP 1135 'Sedimentary basin dynamics' (grants Kr2073/1 and Ta427/1).

REFERENCES

Allen, P.A. & Allen, J.R. 1990. *Basin Analysis – Principles and Applications*. Blackwell, Oxford.

Aminzadeh, F. 1987. *Pattern Recognition and Image Processing*. Geophysical Press, London.

Baldschuhn, R., Frisch, U. & Kockel, F. 1996. *Geotektonischer Atlas von Nordwest-Deutschland, 1:300.000*. BGR, Hannover, Germany.

Betz, D., Führer, F., Greiner, G. & Plein, E. 1987. Evolution of the Lower Saxony Basin. *Tectonophysics*, **137**, 127–170.

Brink, H.J., Dürschner, H. & Trappe, H. 1992. Some aspects of the late and post-Variscan development of the Northwestern German Basin. *Tectonophysics*, **207**, 65–95.

Deutsch, C.V. & Journel, A.G. 1992. *GSLIB – Geostatistical Software Library and User's Guide*. Oxford University Press, New York.

Ekstrom, M.P., Dahan, C.A., Chen, M.Y., Lloyd, P.M. & Rossi, D.J. 1987. Formation imaging with microelectrical scanning arrays. *The Log Analyst*, **28**, 294–306.

Goodall, T.M., Moller, N.K. & Ronningsland, T.M. 1998. The integration of electrical image logs with core data for improved sedimentological interpretation. *In:* Harvey, P.K. & Lovell, M.A. (eds) *Core-Log Integration*. Geological Society, London, Special Publications, **136**, 237–248.

Kockel, F. 2002. Rifting processes in NW Germany and the German North Sea sector. *Netherlands Journal of Geosciences/Geologie en Mijnbouw*, **81**, 149–158.

Kossow, D. & Krawczyk, C.M. 2002. Structure and quantification of factors controlling the evolution of the inverted NE German Basin. *Marine and Petroleum Geology*, **19**, 601–618.

Kossow, D., Krawczyk, C., McCann, T., Strecker, M. & Negendank, J.F.W. 2000. Style and evolution of salt pillows and related structures in the northern part of the Northeast German Basin. *International Journal of Earth Sciences*, **89**, 652–664.

Krawczyk, C.M., Stiller, M. & DEKORP-BASIN Research Group. 1999. Reflection seismic constraints on Paleozoic crustal structure and Moho beneath the NE German Basin. *Tectonophysics*, **314**, 241–253.

Lohr, T., Krawczyk, C.M., Tanner, D.C. *et al.* 2007. Strain partitioning due to salt – insights from interpretation of a 3D seismic data set in the NW German Basin. *Basin Research*, **19**, 579–597.

Marrett, R. & Allmendinger, R.W. 1991. Estimates of strain due to brittle faulting: sampling of fault populations. *Journal of Structural Geology*, **13**, 735–738.

Mauthe, G. 2003. Kompartmentbildende Verwerfungen infolge Kataklase (Rotliegend, NW-Deutschland). *Erdöl Erdgas Kohle*, **119**, 12–17.

Pharaoh, T.C. 1999. Palaeozoic terranes and their lithospheric boundaries within the Trans-European Suture Zone (TESZ): a review. *Tectonophysics*, **314**, 17–41.

Plein, E. 1995. *Norddeutsches Rotliegendbecken – Rotliegend-Monographie Teil II*. Senckenbergische Naturforschende Gesellschaft, Frankfurt/M.

Scheck, M. & Bayer, U. 1999. Evolution of the Northeast German Basin – inferences from a 3-D structural model and subsidence analysis. *Tectonophysics*, **313**, 145–169.

Scholz, C.H. & Cowie, P.A. 1990. Determination of total strain from faulting using slip measurements. *Nature*, **346**, 837–839.

Schwab, G., Benek, R., Jubitz, K.-B. & Teschke, H.-J. 1982. Intraplattentektonik und Bildungsprozeß der Mitteleuropäischen Senke. *Zeitschrift für geologische Wissenschaften*, **10**, 397–413.

Tanner, B. & Meissner, R. 1996. Caledonian deformation upon southwest Baltica and its tectonic implications: Alternatives and consequences. *Tectonics*, **15**, 803–812.

Trappe, H. & Hellmich, C. 2003. Seismic volume attributes for fracture analysis. *In:* Ameen, M. (ed.) *Fracture and In-Situ Characterization of Hydrocarbon Reservoirs*. Geological Society, London, Special Publications, **209**, 65–75.

Trappe, H., Hellmich, C. & Foell, M. 2000. Potential power in the application of seismic volume attributes. *First Break*, **18**, 397–402.

Walsh, J.J., Watterson, J., Heath, A., Gillespie, P.A. & Childs, C. 1998. Assessment of the effects of sub-seismic faults on bulk permeabilities of reservoir properties. *In:* Coward, M.P., Daltaban, T.S. & Johnson, H. (eds) *Structural Geology in Reservoir Characterization*. Geological Society, London, Special Publications, **127**, 99–114.

Yilmaz, Ö. 1987. *Seismic Data Processing. Investigations in Geophysics. Volume 2*. Society of Exploration Geophysicists, Tulsa, OK.

Ziegler, P. 1990. *Geological Atlas of Western and Central Europe*. Shell, The Hague.

Received 21 March 2007; revised typescript accepted 20 March 2008.